SLAC–PUB–6403
PITHA 93/43
December 1993
T/E
hep-ph/9312210

Tracing CP violation in the production of top quark pairs by multiple TeV proton–proton collisions [1]

Werner Bernreuther

Institut f. Theoretische Physik
Physikzentrum, RWTH Aachen
52056 Aachen, Germany

Arnd Brandenburg [2]

Stanford Linear Accelerator Center, P.O. Box 4349
Stanford, California 94309, USA

Abstract

We investigate the possibilities of searching for non-standard CP violation in $pp \to t\bar{t}X$ at multiple TeV collision energies. A general kinematic analysis of the underlying partonic production processes $gg \to t\bar{t}$ and $q\bar{q} \to t\bar{t}$ in terms of their density matrices is given. We evaluate the CP-violating parts of these matrices in two-Higgs doublet extensions of the standard model (SM) and give results for CP asymmetries at the parton level. We show that these asymmetries can be traced by measuring suitable observables constructed from energies and momenta of the decay products of t and $\bar{t}$. We find CP-violating effects to be of the order of 10^{-3} and show that possible contaminations induced by SM interactions are savely below the expected signals.

[1] Work supported by the Department of Energy, contract DE-AC03-76SF00515
[2] Supported by Max Kade Foundation

1 Introduction

A high energy and high luminosity proton-proton collider, such as the planned Large Hadron Collider (LHC) at CERN, would be capable of producing millions of top and antitop quarks. This would offer the unique possiblity to explore in detail the physics of these quarks – which have not been discovered yet, but for whose existence there is indirect evidence [1]. Specifically, since the top is known to be heavy, $m_t > 113$ GeV [2], precision studies based on large samples of $t\bar{t}$ events may serve as a probe, through sizeable top-Yukawa couplings, to the electroweak symmetry breaking sector (Higgs sector for short). This sector may have a richer structure than the one conceived in the standard model (SM) — as is the case in many of its extensions. As a consequence a number of new phenomena may exist. A particularly intriguing one is a new "source" of CP violation provided by the Higgs sector[1] which is unrelated to the Kobayashi-Maskawa phase [3]. This is possible already in the two-Higgs doublet extensions of the SM [5]–[7]: here neutral Higgs boson exchange leads to CP-violating effects in fermionic amplitudes, and these effects would show up most pronouncedly in reactions involving top quarks [8]–[11]. The subject of this paper is to investigate in detail[2] the manifestation and the magnitude of neutral Higgs particle CP violation in $pp \to t\bar{t}X$. (For other studies on CP violation in top quark production and decay see [12]–[25].)

The outline of our paper is as follows: In section 2 we give a general kinematic analysis of the reactions $gg \to t\bar{t}$ and $q\bar{q} \to t\bar{t}$ which are the leading partonic processes in $pp \to t\bar{t}X$. We study these reactions in terms of their production density matrices and describe the properties of these matrices under various symmetry transformations including CP transformations. In section 3 we evaluate the CP-violating parts of the density matrices in a specific model, namely the two-Higgs doublet extensions of the SM with CP-nonconserving neutral Higgs boson exchange. Correlations which are sensitive to CP violation at the parton level are identified and results for their expectation values are presented. In section 4 we show that these CP asymmetries can be traced in $pp \to t\bar{t}X$ by looking at simple observables which involve energies and/or momenta of the decay products of t and $\bar{t}$. Moreover, possible contaminations by CP-conserving interactions are discussed and shown to be much smaller than the expected signals. In an appendix we list the analytic results of our calculations.

[1] This source was shown to be of interest in attempts to explain the cosmological baryon asymmetry [4].

[2] A short account of our work was given in [11].

2 Production density matrices for $gg \to t\bar{t}$ and $q\bar{q} \to t\bar{t}$

Because a heavy top has an extremely short lifetime ($\tau_t < 10^{-23} s$ if $m_t > 100$ GeV), the polarization of and spin–spin correlations between t and $\bar{t}$ are not severely diluted by hadronization [34]. These are "good" observables in the sense that effects involving the spins of t and $\bar{t}$ can be treated perturbatively. Therefore we will discuss the reaction $pp \to t\bar{t}X$, respectively the underlying partonic processes in terms of production density matrices. We will consider only unpolarized pp collisions. At LHC energies $t\bar{t}$ pairs are produced mainly by gluon gluon fusion. This reaction dominates over quark antiquark annihilation into $t\bar{t}$. We will first discuss the (unnormalized) production density matrix for the reaction $g(p_1) + g(p_2) \to t(k_1) + \bar{t}(k_2)$ in the gluon–gluon center of mass system. It is defined by

$$R^g_{\alpha_1\alpha_2,\ \beta_1\beta_2}(\mathbf{p},\mathbf{k}) = N_g^{-1} \sum_{\text{colors,gluon spin}} \langle t(k_1,\alpha_1), \bar{t}(k_2,\beta_1)|\mathcal{T}|g(p_1),g(p_2)\rangle^* \langle t(k_1,\alpha_2), \bar{t}(k_2,\beta_2)|\mathcal{T}|g(p_1),g(p_2)\rangle \quad (2.1)$$

where $\alpha,\ \beta$ are spin indices, $\mathbf{p} = \mathbf{p}_1,\ \mathbf{k} = \mathbf{k}_1$ and $N_g = 256$. We sum here over the gluon spins and colors since we are only interested in analysing the polarizations of the t and $\bar{t}$ and their spin–spin correlations. The matrix R^g can be decomposed in the spin spaces of t and $\bar{t}$ as follows:

$$R^g = A^g \mathbb{1} \otimes \mathbb{1} + B_i^{g+} \sigma^i \otimes \mathbb{1} + B_i^{g-} \mathbb{1} \otimes \sigma^i + C_{ij}^g \sigma^i \otimes \sigma^j. \quad (2.2)$$

The first (second) factor in the tensor products of the 2×2 unit matrix $\mathbb{1}$ and of the Pauli matrices σ^i refers to the t ($\bar{t}$) spin space.

Because of rotational invariance, the functions $B_i^{g\pm}$ and C_{ij} can be further decomposed:

$$\begin{aligned} B_i^{g\pm} = \quad & b_{g1}^{\pm} \hat{p}_i + b_{g2}^{\pm} \hat{k}_i + b_{g3}^{\pm} \hat{n}_i \\ C_{ij} = \quad & c_{g0}\delta_{ij} + \epsilon_{ij\ell}(c_{g1}\hat{p}_\ell + c_{g2}\hat{k}_\ell + c_{g3}\hat{n}_\ell) \\ & + c_{g4}\hat{p}_i\hat{p}_j + c_{g5}\hat{k}_i\hat{k}_j + c_{g6}(\hat{p}_i\hat{k}_j + \hat{p}_j\hat{k}_i) \\ & + c_{g7}(\hat{p}_i\hat{n}_j + \hat{p}_j\hat{n}_i) + c_{g8}(\hat{k}_i\hat{n}_j + \hat{k}_j\hat{n}_i). \end{aligned} \quad (2.3)$$

Here the hat denotes a unit vector and $\mathbf{n} = \mathbf{p} \times \mathbf{k}$. The structure functions A^g, $b_{gi}^{\pm}$ and c_{gi} depend only on $\hat{s} = (p_1 + p_2)^2$ and on the cosine of the scattering angle, $z = \hat{\mathbf{p}} \cdot \hat{\mathbf{k}}$.

Next we discuss the properties of R^g under various symmetry transformations. Since the initial gg state is Bose symmetric, R^g must satisfy

$$R^g(-\mathbf{p},\mathbf{k}) = R^g(\mathbf{p},\mathbf{k}). \tag{2.4}$$

The initial gg state, when averaged over colors and spins, is a CP eigenstate in its center of mass system. It is therefore possible to classify the individual terms in R^g according to their CP transformation properties. If the interactions were CP-invariant, the matrix R^g would have to satisfy

$$R^g_{\beta_1\beta_2,\ \alpha_1\alpha_2}(\mathbf{p},\mathbf{k}) \ = R^g_{\alpha_1\alpha_2,\ \beta_1\beta_2}(\mathbf{p},\mathbf{k}). \tag{2.5}$$

In table 1 we give a complete list of the transformation properties of the structure functions under P, CP, and exchange of the initial gluons ("Bose"). It is also instructive to collect the properties of these functions under time reversal (T) and CPT transformations neglecting, just for this purpose, non-hermitean parts of the scattering matrix. To give an example, table 1 is then to be read as follows: for a T-invariant interaction one has $b^{\pm}_{g3}(z) = -b^{\pm}_{g3}(z)$, i.e., $b^{\pm}_{g3} = 0$ only at the Born level, whereas at higher orders absorptive parts render this function non-zero.
Because of Bose symmetry, the structure functions $A^g,\ b^{\pm}_{g2},\ c_{g0},\ c_{g2},\ c_{g4},\ c_{g5}$ and c_{g7} are even functions of z, the other functions are odd in z.

The contributions to R^g can be decomposed into a CP–even and a CP–odd part:

$$R^g = R^g_{\rm even} + R^g_{CP}. \tag{2.6}$$

As can be read off from table 1, the CP–even term $R^g_{\rm even}$ in general has the following structure:

$$\begin{aligned} R^g_{\rm even} = \ & A^g \mathbb{1}\otimes\mathbb{1} + (b^{\rm even}_{g1}\hat{p}_i + b^{\rm even}_{g2}\hat{k}_i + b^{\rm even}_{g3}\hat{n}_i)(\sigma^i\otimes\mathbb{1} + \mathbb{1}\otimes\sigma^i) \\ & +(c_{g0}\delta_{ij} + c_{g4}\hat{p}_i\hat{p}_j + c_{g5}\hat{k}_i\hat{k}_j + c_{g6}(\hat{p}_i\hat{k}_j + \hat{p}_j\hat{k}_i) \\ & +c_{g7}(\hat{p}_i\hat{n}_j + \hat{p}_j\hat{n}_i) + c_{g8}(\hat{k}_i\hat{n}_j + \hat{k}_j\hat{n}_i))\sigma^i\otimes\sigma^j. \end{aligned} \tag{2.7}$$

Nonzero $b^{\rm even}_{g1},\ b^{\rm even}_{g2},\ c_{g7},\ c_{g8}$ can be induced only by parity-violating interactions, $c_{g7},\ c_{g8}$ need in addition absorptive parts in the scattering amplitude when the interactions are CPT-invariant. The structure function $b^{\rm even}_{g3}$ can only get contributions from absorptive parts induced by parity-invariant interactions.
The CP–odd term R^g_{CP} reads

$$\begin{aligned} R^g_{CP} = \ & (b^{CP}_{g1}\hat{p}_i + b^{CP}_{g2}\hat{k}_i + b^{CP}_{g3}\hat{n}_i)(\sigma^i\otimes\mathbb{1} - \mathbb{1}\otimes\sigma^i) \\ & +\epsilon_{ijk}(c_{g1}\hat{p}_i + c_{g2}\hat{k}_i + c_{g3}\hat{n}_i)\sigma^j\otimes\sigma^k. \end{aligned} \tag{2.8}$$

CP-violating interactions which are also parity-violating can give contributions to b_{g1}^{CP}, b_{g2}^{CP}, c_{g1}, c_{g2}. Nonzero b_{g1}^{CP}, b_{g2}^{CP} require in addition absorptive parts. C- and CP-violating interactions can induce non–vanishing structure functions b_{g3}^{CP}, c_{g3}, where $c_{g3} \neq 0$ requires in addition absorptive parts.

The above discussion of the transformation properties of the structure functions holds to all orders of pertubation theory.

The production density matrix R^q for $q\bar{q} \to t\bar{t}$ is defined in complete analogy to (2.1) as

$$R^q_{\alpha_1\alpha_2,\ \beta_1\beta_2}(\mathbf{p},\mathbf{k}) = N_q^{-1} \sum_{\text{colors},q\bar{q}\ \text{spins}} \langle t(k_1,\alpha_1),\bar{t}(k_2,\beta_1)|\mathcal{T}|q(p_1),q(p_2)\rangle^* \langle t(k_1,\alpha_2),\bar{t}(k_2,\beta_2)|\mathcal{T}|q(p_1),q(p_2)\rangle, \quad (2.9)$$

where $N_q = 36$. The decomposition of R^q in the spin spaces of t and $\bar{t}$ is exactly the same as for R^g (equ. (2.2) , (2.3)) as is the splitting into CP–even and odd terms (equ. (2.6)– (2.8)). The transformation properties of the structure functions $A^q, \ldots, c_{q8}$ of R^q are the same as the respective ones for $A^g, \ldots, c_{g8}$ of R^g given in table 1. Thus all conclusions derived from these transformation properties — except those from Bose symmetry, of course — are also valid for the structure functions of R^q.

3 CP violation and density matrices in two-Higgs doublet models

Up to now our discussion has been independent of any specific model. Suffice it to say that the Kobayashi-Maskawa mechanism of CP violation [3] induces only tiny effects in the flavor-diagonal reactions of sect. 2. In the following we will concentrate on CP-violating effects generated by two–Higgs doublet extensions of the SM with CP violation in the scalar potential [6]. We briefly recall the features of these models relevant for us. CP violation in the scalar potential induces mixing of CP–even and –odd scalars, thus leading to three physical mass eigenstates $|\varphi_j\rangle$ $(j = 1, 2, 3)$ with no definite CP parity. That means, these bosons couple both to scalar and pseudoscalar fermionic currents. For the top quark these couplings are (in the notation of [8]):

$$\mathcal{L}_Y = -(\sqrt{2}G_F)^{1/2} \sum_{j=1}^{3} (a_{jt} m_t \bar{t}t + \tilde{a}_{jt} m_t \bar{t} i\gamma_5 t)\varphi_j, \quad (3.1)$$

where G_F is Fermi's constant, m_t is the top mass,

$$a_{jt} = d_{2j}/\sin\beta, \quad \tilde{a}_{jt} = -d_{3j}\cot\beta, \quad (3.2)$$

$\tan\beta = v_2/v_1$ is the ratio of vacuum expectation values of the two doublets, and d_{2j}, d_{3j} are the matrix elements of a 3×3 orthogonal matrix which describes the

mixing of the neutral states [8]. In the following we assume that the couplings and masses of $\varphi_{2,3}$ are such that their effect on all quantities discussed below is negligible. Then the measure of CP violation generated by $\varphi \equiv \varphi_1$ exchange in flavor–diagonal reactions like $gg \to t\bar{t},\ q\bar{q} \to t\bar{t}$ is

$$\gamma_{CP} \equiv -a\tilde{a} = d_{21}d_{31}\cot\beta/\sin\beta, \tag{3.3}$$

where we have put $a = a_{1t},\ \tilde{a} = \tilde{a}_{1t}$. So far, data from low energy phenomenology, in particular the experimental upper bounds on the electric dipole moments of the neutron [26] and of the electron [27] do not severely constrain this parameter: γ_{CP} may be of order one. We note here that the couplings of the φ_j to quarks and leptons induce CP violation already at the Born level. The especially interesting case of a Higgs boson φ decaying into $t\bar{t}$ was shown in [11] to lead to CP-violating spin–spin correlations which may be as large as 0.5. (For other discussions of the CP properties of neutral Higgs bosons see [28]–[33].)

We will now discuss the structure of the matrices R^g_{CP} and R^q_{CP} in these models. The Higgs boson contributions to the processes $gg \to t\bar{t}$ and $q\bar{q} \to t\bar{t}$ discussed in section 2 are shown, together with the leading SM diagrams, in figs. 1, 2. Since the CP-nonconserving neutral Higgs exchange is, in particular, parity-violating, the relations

$$R^{g(q)}_{CP}(-\mathbf{p}, -\mathbf{k}) = -R^{g(q)}_{CP}(\mathbf{p}, \mathbf{k}) \tag{3.4}$$

hold as long as R_{CP} results from interference of these Higgs exchange amplitudes with amplitudes from parity-invariant interactions. This forces b^{CP}_{g3}, c_{g3} and b^{CP}_{q3}, c_{q3} to be zero in these models. Furthermore, the virtual intermediate gluon produced by annihilation of unpolarized q and $\bar{q}$ cannot have a vector polarization. Thus the contributions of fig. 2 to R^q are invariant with respect to the substitution $\mathbf{p} = \mathbf{p}_1 \to -\mathbf{p}$. Hence the structures of R^g_{CP} and R^q_{CP} are the same; the functions b^{CP}_{g1}, c_{g1}, b^{CP}_{q1}, c_{q1} of eqn. (2.8) are odd under $z \to -z$, whereas b^{CP}_{g2}, c_{g2}, b^{CP}_{q2}, c_{q2} are even functions of z.

The explicit results for the matrices R^g and R^q evaluated from the diagrams of fig. 1, 2, respectively, are given in the appendix. The width of φ must be taken into account in the calculation of R^g if $\varphi > 2m_t$, since in that case the contribution from fig. 1h can become resonant. Because for $\varphi > 2m_t$ the width of φ is not very small as compared to its mass it is important to note that the narrow width approximation cannot be applied in this case.

In view of the above discussion it is now very easy to identify the correlations at the parton level which trace the various CP–odd parts of the production density matrices. The expectation value of an observable $\mathcal{O}$ for the respective parton reactions is defined as

$$\langle\mathcal{O}\rangle_i = \frac{\int_{-1}^{1} dz \mathrm{tr}(R^i\mathcal{O})}{4\int_{-1}^{1} dz A^i} \qquad (i = g, q) \tag{3.5}$$

Contributions of the functions $b^{CP}_{g1,g2}$, $b^{CP}_{q1,q2}$ are picked up by taking expectation values of

$$\hat{\mathbf{k}} \cdot (\mathbf{s}_+ - \mathbf{s}_-) f_e(z), \tag{3.6}$$

or

$$\hat{\mathbf{p}} \cdot (\mathbf{s}_+ - \mathbf{s}_-) f_o(z), \tag{3.7}$$

or linear combinations thereof, where $\mathbf{s}_+$, $\mathbf{s}_-$ are the spin operators of t and $\bar{t}$, respectively, $f_e(z)$ is an even function of z and $f_o(z)$ is odd in z. One has for example

$$\langle \hat{\mathbf{k}} \cdot (\mathbf{s}_+ - \mathbf{s}_-) \rangle_g = \frac{4 \int_{-1}^{1} dz (z b^{CP}_{g1} + b^{CP}_{g2})}{4 \int_{-1}^{1} dz A^g}, \tag{3.8}$$

and likewise for $\langle \hat{\mathbf{k}} \cdot (\mathbf{s}_+ - \mathbf{s}_-) \rangle_q$.

The result for the basic longitudinal polarization asymmetry $\langle \hat{\mathbf{k}} \cdot (\mathbf{s}_+ - \mathbf{s}_-) \rangle_g$ is plotted in fig. 3 as a function of the parton CM energy for $m_t = 150$ GeV and two values of the Higgs boson mass: The dashed curve corresponds to $m_\varphi = 100$ GeV and $\gamma_{CP} = 1$. For m_φ of the order of $2m_t$ or larger, the shape of the resulting graph depends, for fixed m_φ, on the strength of the Higgs couplings a, $\tilde{a}$ and on the couplings to W^+W^-, ZZ determining the width of the φ. (See eqn. (A.10) for details.) For the solid line we have chosen $m_\varphi = 350$ GeV, $|a| = |\tilde{a}| = \gamma_{CP} = 1$ and $\Gamma_\varphi = 47$ GeV. The asymmetry $\langle \hat{\mathbf{k}} \cdot (\mathbf{s}_- - \mathbf{s}_+) \rangle$ corresponds to the asymmetry $\Delta N_{LR} = [N(t_L \bar{t}_L) - N(t_R \bar{t}_R)]/(\text{all } t\bar{t})$ studied in [10]. We reproduce the numerical results of [10] for ΔN_{LR} if we neglect Γ_φ and use $\gamma_{CP} = 1/\sqrt{2}$ which corresponds to the parameter $\mathrm{Im}(A^2) = \sqrt{2}$ used in [10].

The functions $c_{g1,g2}$, $c_{q1,q2}$ generate nonzero expectation values of the triple product correlations

$$\hat{\mathbf{k}} \cdot (\mathbf{s}_+ \times \mathbf{s}_-) h_e(z), \tag{3.9}$$

$$\hat{\mathbf{p}} \cdot (\mathbf{s}_+ \times \mathbf{s}_-) h_o(z), \tag{3.10}$$

and of their linear combinations, where h_e and h_o are even and odd functions of z, respectively. For example,

$$\langle \hat{\mathbf{k}} \cdot (\mathbf{s}_+ \times \mathbf{s}_-) \rangle_g = \frac{2 \int_{-1}^{1} dz (z c_{g1} + c_{g2})}{4 \int_{-1}^{1} dz A^g}. \tag{3.11}$$

In fig. 4 we plot this basic CP–odd and T–odd spin–spin correlation with the same choice of parameters as in fig. 3. It reaches values of up to about two percent.

For completeness, we show in figs. 5 and 6 the expectation values $\langle \hat{\mathbf{k}} \cdot (\mathbf{s}_+ - \mathbf{s}_-) \rangle_q$ and $\langle \hat{\mathbf{k}} \cdot (\mathbf{s}_+ \times \mathbf{s}_-) \rangle_q$, respectively, again for the same choice of parameters as in fig. 3. Here the CP asymmetries get smaller with growing Higgs masses.

4 CP observables for $pp \to t\bar{t}X$

The CP-violating spin-momentum correlations for t and $\bar{t}$ of the previous section must be traced in the final states into which t and $\bar{t}$ decay. In this section we discuss a few observables which allow to do this. The charged lepton from $t \to Wb \to \ell^+\nu_\ell b$ is an efficient analyzer of the top spin [35]. We will therefore conider only decay chains where at least one of the top quarks decays semileptonically. We shall use the SM decay density matrices as given in [16, 18].

Observables in $pp \to t\bar{t}X$ cannot be classified as being even or odd with respect to CP, because the initial state is not a CP eigenstate. However, they can be classified as being T–even or T–odd (i.e. even or odd under reflection of momenta and spins). Their expectation values will in general be contaminated by contributions from CP-conserving interactions.

The asymmetries in the t and $\bar{t}$ polarizations in the production plane, as given in eqns. (3.6) and (3.7), translate into T–even observables formed by energies and/or momenta of the final states. As an example, we have investigated the expectation values of the following two observables (another one was given in [10]):

$$A_1 = E_+ - E_- \tag{4.1}$$

$$A_2 = \mathbf{k}_{\bar{t}} \cdot \boldsymbol{\ell}^+ - \mathbf{k}_t \cdot \boldsymbol{\ell}^-. \tag{4.2}$$

Here $E_\pm$, $\boldsymbol{\ell}^\pm$ are the energies and momenta of the leptons in $t \to \ell^+\nu_\ell b$ and $\bar{t} \to \ell^-\bar{\nu}_\ell\bar{b}$ in the laboratory frame and $\mathbf{k}_{t(\bar{t})}$ is the top (antitop) momentum in this system.

To measure A_2, one has to select events where the t decays leptonically and the $\bar{t}$ hadronically, which in principle allow to reconstruct the $\bar{t}$ momentum [36], and vice versa. We will give explicit expressions for the expectation values of A_1 and A_2 below when we discuss contaminations by CP-conserving interactions. In calculating these expectation values we have used the narrow width approximation for the top: because the top width is much smaller than its mass (in view of the experimental upper bound on m_t which is of the order of 200 GeV), the approximation of the on–shell production of t and $\bar{t}$ followed by their weak decays yields a good description of the reactions considered here. We also neglected CP violation in the decays of t and $\bar{t}$ (for comments on this, see [11]). For the parton distributions entering the calculation of expectation values in pp collisions we have used the parametrization of [37]. In order to assess the statistical sensitivity of the observables A_1 and A_2, we have computed the signal–to–noise ratios $\langle A_i\rangle/\Delta A_i$ $(i = 1, 2)$ for Higgs masses 100 GeV $\leq m_\varphi \leq$ 450 GeV both for $\sqrt{s} = 15$ TeV (LHC) and $\sqrt{s} = 40$ TeV. Here $\Delta A_i = \sqrt{\langle A_i^2\rangle - \langle A_i\rangle^2}$ denotes the width of the distribution of A_i. We present our results in figs. 7 and 8 for the same parameter set as used in calculating the partonic asymmetries, that is, $a = -\tilde{a} = 1, \hat{g}_{VV} = 1$ (for the definition of $\hat{g}_{VV}$ see appendix, eqn. (A.9)). We integrate here over the whole phase space. Both observables have signal–to–noise ratios of order 10^{-3}. LHC offers larger effects due to the fact that $\Delta A_{1,2}$ is larger for $\sqrt{s}$= 40 TeV.

If both t and $\bar{t}$ decay leptonically, one can look at the T–odd observable

$$T_2 = (\mathbf{b} - \bar{\mathbf{b}}) \cdot (\boldsymbol{\ell}^+ \times \boldsymbol{\ell}^-) \tag{4.3}$$

where $\mathbf{b}$, $\bar{\mathbf{b}}$ denote the momenta of the b and $\bar{b}$ jets in the laboratory frame. (This observable was also discussed in [11].) The expectation value of T_2 traces the spin–spin correlations of (3.9) and (3.10). In fig. 9 we show the signal–to–noise ratio as a function of the Higgs mass for this observable, again with the same choice of parameters as for $A_{1,2}$. The effect is also of the order of 10^{-3}.

We will now discuss in some detail possible contaminations of the observables $A_{1,2}$ and T_2 due to CP-conserving interactions. Such contaminations arise in particular because the pp initial state is not a CP eigenstate. One can give general arguments why these contaminations should be small. Most importantly, the dominant subprocess is gluon fusion which does not induce any CP-conserving contributions to our observables (cf. [11] and below). Furthermore, T–odd observables like T_2 do not receive contributions from CP-invariant interactions at the Born level but only from absorptive parts. The main background in this case comes from order α_s^3 and order $\alpha_s^2 \alpha_{\rm weak}$ absorptive parts in $q\bar{q} \to t\bar{t}$ which generate nonzero functions $b_3^{\rm even}$ in R^q. However, numerical simulations show that these contributions are smaller than 10^{-6}, i.e. about three orders of magnitude smaller than the signal shown in fig. 9. Potentially more dangerous are CP–even contributions to A_1 and A_2, because, as will be shown below, they can already be generated by weak interactions at the Born level.

Integrating over the whole phase space we can actually give explicit analytic formulae for the expectation values of A_1 and A_2 in terms of the structure functions. This is very illuminating for identifying possible contaminations. We have carried out our calculations within the naive parton model (which neglects intrinsic transverse momenta of the incoming partons) and restricted ourselves again to gg and $q\bar{q}$ initial states. Furthermore, we have used the narrow width approximation desribed above and have taken into account only the SM decays of t and $\bar{t}$. Then we find:

$$\begin{aligned}
\langle A_1 \rangle \;=\; & \frac{1}{\sigma}\frac{1}{2s}\frac{g(m_W^2/m_t^2)}{4\pi} \\
& \Big\{ \int_0^1 dx_1 \frac{N_g^p(x_1)}{x_1} \int_0^1 dx_2 \frac{N_g^p(x_2)}{x_2} \int_{-1}^1 dz\beta \frac{x_1+x_2}{2\sqrt{x_1x_2}} \frac{E_1}{3}(z b_{g1}^{CP} + b_{g2}^{CP}) \\
& + 2\int_0^1 dx_1 \frac{N_q^p(x_1)}{x_1} \int_0^1 dx_2 \frac{N_{\bar{q}}^p(x_2)}{x_2} \int_{-1}^1 dz\beta \Big[\frac{x_1+x_2}{2\sqrt{x_1x_2}} \frac{E_1}{3}(z b_{q1}^{CP} + b_{q2}^{CP}) \\
& + \frac{x_1-x_2}{2\sqrt{x_1x_2}} \Big(E_1 \beta z A^q + \frac{1}{3}([(1-z^2)m_t + z^2 E_1] b_{q1}^{\rm even} + E_1 z b_{q2}^{\rm even}) \Big) \Big] \Big\},
\end{aligned} \tag{4.4}$$

$$
\begin{aligned}
\langle A_2 \rangle \;=\; & \frac{1}{\sigma}\frac{1}{2s}\frac{g(m_W^2/m_t^2)}{4\pi} \\
& \Big\{ \int_0^1 dx_1 \frac{N_g^p(x_1)}{x_1} \int_0^1 dx_2 \frac{N_g^p(x_2)}{x_2} \int_{-1}^1 dz \beta \Big[-\frac{E_1^2\beta}{3}(z b_{g1}^{CP} + b_{g2}^{CP}) \\
& + \frac{(x_1-x_2)^2}{4x_1x_2}\frac{E_1\beta}{3}(1-z^2)((E_1-m_t) z b_{g1}^{CP} + E_1 b_{g2}^{CP}) \Big] \\
& + 2\int_0^1 dx_1 \frac{N_q^p(x_1)}{x_1} \int_0^1 dx_2 \frac{N_{\bar q}^p(x_2)}{x_2} \int_{-1}^1 dz \beta \Big[-\frac{E_1^2\beta}{3}(z b_{q1}^{CP} + b_{q2}^{CP}) \\
& + \frac{(x_1-x_2)^2}{4x_1x_2}\frac{E_1\beta}{3}(1-z^2)[(E_1-m_t) z b_{q1}^{CP} + E_1 b_{q2}^{CP}] \\
& + \frac{x_1^2-x_2^2}{4x_1x_2}\frac{m_t}{3}([(1-z^2)E_1 + z^2 m_t] b_{q1}^{\rm even} + m_t z b_{q2}^{\rm even}) \Big] \Big\}. \qquad (4.5)
\end{aligned}
$$

Here σ is the total cross section for $pp \to t\bar{t}X$, s is the pp collision energy squared, $g(y) = (1+2y+3y^2)/(2+4y)$, N_g^p, $N_{q(\bar q)}^p$ denote the gluon and quark (antiquark) distribution functions of the proton, E_1 is the energy of the top quark in the partonic CM and $\beta = (1-m_t^2/E_1^2)^{1/2}$.

Equations (4.4) and (4.5) exhibit several interesting features:
- One can see explicitly that gluon fusion generates no CP-even contributions to the observables.
- Quark–antiquark annihilation produces several contaminations: In $\langle A_1 \rangle$ a term $\sim z A^q(z)$ appears which, after integrating over z, is nonzero only if $A^q(z)$ has a part which is odd in z; that is, if $q\bar q \to t\bar t$ has a forward–backward asymmetry. Such an asymmetry is induced in order α_s^3. (In [10] this potential source of contaminations was discussed.) Possibly more important are the terms $b_{q1}^{\rm even}$ and $b_{q2}^{\rm even}$ which appear in both expectation values above because these terms can be generated at the Born level via $q\bar q \to Z \to t\bar t$. We calculated their contributions and found that for both observables they are suppressed by more than two orders of magnitude in comparison to the signals shown in figs. 7 and 8.

A future multiple TeV and high luminosity collider like the LHC has the potential of producing more than 10^7 $t\bar t$ pairs. If it were for statistics alone detection of effects of a few permil which we found might be feasible. More detailed (Monte Carlo) studies including judicious choices of phase space cuts are required in order to explore the possiblity of enhancing the signals by some factor. A crucial issue will eventually be whether detector effects can be kept at the level of 10^{-3}.

5 Conclusions

In this article we have studied the possibility of detecting CP violation in top quark pair production at future hadron colliders. We have given a general kinematic analysis of the underlying dominant partonic subprocesses and identified the relevant CP asymmetries at the parton level. We have further computed these asymmetries in two-Higgs doublet extensions of the SM where CP violation is generated through neutral Higgs boson exchange. Whereas at the parton level these models can induce asymmetries of the order of a few percent, realistic observables built up from energies and/or momenta of the final states into which the top quarks decay give signal–to–noise ratios of up to a few $\times 10^{-3}$. Contaminations by CP-conserving interactions were shown to be much smaller than the signals. Since the issue of CP violation is of fundamental interest detailed investigations of the experimental feasibility of an observation of these effects would certainly be worthwhile.

Acknowledgments

A. B. would like to thank the SLAC theory group for the hospitality extended to him.

Appendix

In this appendix we list our analytic results for the structure functions of the $t\bar{t}$ spin density matrix R^g defined in equ. (2.1)–(2.3) and decomposed into CP–even and CP–odd parts in equ. (2.6)–(2.8) and also the corresponding functions in R^q defined in (2.9). All calculations are carried out in the two-Higgs doublet extensions of the SM described in section 3. The relevant Feynman diagrams are shown in figures 1a–h for the process $gg \to t\bar{t}$ and in figures 2a,b for $q\bar{q} \to t\bar{t}$.

R^q is obtained very easily: The CP–even part is determined to good approximation by the Born diagram fig. 2a, whereas R^q_{CP} results from the interference of fig. 2b (with couplings $a\tilde{a} = -\gamma_{CP}$) with fig. 2a. The nonzero CP–even structure functions of R^q read:

$$\begin{aligned} A^q &= \frac{g_s^4(\beta^2(z^2-1)+2)}{18} \\ c_{q0} &= \frac{g_s^4\beta^2(z^2-1)}{18} \\ c_{q4} &= \frac{g_s^4}{9} \\ c_{q5} &= \frac{g_s^4\beta^2}{9}\Big(\frac{\beta^2 z^2 E_1^2}{(E_1+m_t)^2}+1\Big) \\ c_{q6} &= \frac{-g_s^4\beta^2 z E_1}{9(E_1+m_t)}. \end{aligned} \tag{A.1}$$

Here and in the following g_s denotes the strong coupling constant, E_1 is the energy of the top in the CM system of the incoming partons and $\beta = \sqrt{1-m_t^2/E_1^2}$. Recall that $z = \hat{\mathbf{p}} \cdot \hat{\mathbf{k}}$.
The CP–odd contributions are:

$$b_{q1}^{CP} = \frac{-m_t^3\sqrt{2}G_F\gamma_{CP}}{8\pi^2}\frac{4g_s^4 E_1\beta z}{9}\mathrm{Im}G(\hat{s}), \tag{A.2}$$

$$b_{q2}^{CP} = \frac{m_t^3\sqrt{2}G_F\gamma_{CP}}{8\pi^2}\frac{4g_s^4 E_1\beta}{9}\Big[\frac{(z^2-1)\beta^2 E_1}{E_1+m_t}+1\Big]\mathrm{Im}G(\hat{s}), \tag{A.3}$$

$$c_{q1} = \frac{m_t^3\sqrt{2}G_F\gamma_{CP}}{8\pi^2}\frac{4g_s^4 E_1\beta z}{9}\mathrm{Re}G(\hat{s}), \tag{A.4}$$

$$c_{q2} = \frac{-m_t^3\sqrt{2}G_F\gamma_{CP}}{8\pi^2}\frac{4g_s^4 E_1\beta}{9}\Big[\frac{(z^2-1)\beta^2 E_1}{E_1+m_t}+1\Big]\mathrm{Re}G(\hat{s}). \tag{A.5}$$

Here G_F is Fermi's constant and

$$G(\hat{s}) = \frac{-(m_\varphi^2 C_0(\hat{s},m_\varphi^2,m_t^2,m_t^2)+B_0(\hat{s},m_t^2,m_t^2)-B_0(m_t^2,m_\varphi^2,m_t^2))}{\hat{s}\beta^2}, \tag{A.6}$$

where

$$C_0(\hat{s}, m_\varphi^2, m_t^2, m_t^2) =$$
$$\int \frac{d^4l}{i\pi^2} \frac{1}{l^2 - m_\varphi^2 + i\epsilon} \frac{1}{(l+k_1)^2 - m_t^2 + i\epsilon} \frac{1}{(l+k_1-p_1-p_2)^2 - m_t^2 + i\epsilon}. \quad \text{(A.7)}$$

is a standard three-point scalar integral which can be reduced to dilogarithms [38]. We note here that for the models of section 3 all structure functions are ultraviolet finite. In particular, the scalar two-point functions B_0 show up in all our results only as differences of the form

$$B_0(q_1^2, m_1^2, m_t^2) - B_0(q_2^2, m_2^2, m_t^2) =$$
$$-\int_0^1 dx \log\Big[\frac{x^2 q_1^2 + x(m_t^2 - m_1^2 - q_1^2) + m_1^2 - i\epsilon}{x^2 q_2^2 + x(m_t^2 - m_2^2 - q_2^2) + m_2^2 - i\epsilon}\Big]. \quad \text{(A.8)}$$

This completes our results for the matrix R^q.

The computation of R^g is more involved since the contribution of fig. 1h becomes resonant if $m_\varphi > 2m_t$. (Fig. 1h actually represents four amplitudes: two CP–conserving ones with couplings a^2 and $\tilde{a}^2$, respectively, and two CP–violating ones with couplings $a\tilde{a}$.) The width of φ must therefore be taken into account in the φ propagator. We compute Γ_φ by summing the partial widths for $\varphi \to W^+W^-$, ZZ, $t\bar{t}$ in the two–Higgs doublet model which contains (3.1). At the Born level only the $CP = +1$ component of φ couples to W^+W^- and ZZ. The couplings are given by the respective SM couplings times the factor

$$\hat{g}_{VV} = (d_{11}\cos\beta + d_{21}\sin\beta). \quad \text{(A.9)}$$

Explicitly,

$$\begin{aligned}
\Gamma_\varphi &= \Gamma_W + \Gamma_Z + \Gamma_t \\
\Gamma_W &= \Theta(m_\varphi - 2m_W)\frac{\hat{g}_{VV}^2 m_\varphi^3 \sqrt{2} G_F \beta_W}{16\pi}\Big[\beta_W^2 + 12\frac{m_W^4}{m_\varphi^4}\Big] \\
\Gamma_Z &= \Theta(m_\varphi - 2m_Z)\frac{\hat{g}_{VV}^2 m_\varphi^3 \sqrt{2} G_F \beta_Z}{8\pi}\Big[\beta_Z^2 + 12\frac{m_Z^4}{m_\varphi^4}\Big] \\
\Gamma_t &= \Theta(m_\varphi - 2m_t)\frac{3 m_\varphi m_t^2 \sqrt{2} G_F \beta_t}{8\pi}(\beta_t^2 a^2 + \tilde{a}^2). \quad \text{(A.10)}
\end{aligned}$$

Here we have used the notation $\beta_{W,Z,t} = (1 - 4m_{W,Z,t}^2/m_\varphi^2)^{1/2}$. In order to incorporate the resonance region we have determined $R^g_{\rm even}$ from the squared Born amplitudes figs. 1a, 1b, the interference of fig. 1a with the CP–even amplitudes of fig. 1h, and the squared amplitudes of fig. 1h. We denote the Born contributions by a lower index "Born" and the other two contributions by a lower index "resonance" in the following. The results for the nonzero structure functions of $R^g_{\rm even}$ are:

$$
\begin{aligned}
A^g &= A^g_{\rm Born} + A^g_{\rm resonance} \\
A^g_{\rm Born} &= \frac{g_s^4\,(7+9\beta^2 z^2)}{192E_1^4\,(-1+\beta^2 z^2)^2}(E_1^4+2E_1^2m_t^2-2m_t^4-2\beta^2E_1^2m_t^2z^2-\beta^4E_1^4z^4) \\
A^g_{\rm resonance} &= \frac{g_s^4}{(\hat{s}-m_\varphi^2)^2+\Gamma_\varphi^2 m_\varphi^2}\Big\{-\frac{1}{16}\frac{m_t^3\sqrt{2}G_F}{8\pi^2}\frac{m_t}{-1+\beta^2z^2} \\
&\quad \Big[2\hat{s}(a^2\beta^4+\tilde{a}^2)[{\rm Re}C_0(\hat{s},m_t^2,m_t^2,m_t^2)(\hat{s}-m_\varphi^2) \\
&\quad +{\rm Im}C_0(\hat{s},m_t^2,m_t^2,m_t^2)\Gamma_\varphi m_\varphi]-4a^2\beta^2(\hat{s}-m_\varphi^2)\Big] \\
&\quad +\frac{3}{32}\left(\frac{m_t^3\sqrt{2}G_F}{8\pi^2}\right)^2\Big[\hat{s}^3(a^2\tilde{a}^2\beta^2+\tilde{a}^4)|C_0(\hat{s},m_t^2,m_t^2,m_t^2)|^2 \\
&\quad +\hat{s}(a^4\beta^2+a^2\tilde{a}^2)|2-\hat{s}\beta^2C_0(\hat{s},m_t^2,m_t^2,m_t^2)|^2\Big]\Big\}, \qquad \text{(A.11)}
\end{aligned}
$$

$$
\begin{aligned}
c_{g0} &= c_{g0,\rm Born} + c_{g0,\rm resonance} \\
c_{g0,\rm Born} &= \frac{-g_s^4(7+9\beta^2z^2)}{192E_1^4(-1+\beta^2z^2)^2}(E_1^4-2E_1^2m_t^2+2m_t^4 \\
&\quad -2\beta^2E_1^4z^2+2\beta^2E_1^2m_t^2z^2+\beta^4E_1^4z^4) \\
c_{g0,\rm resonance} &= \frac{g_s^4}{(\hat{s}-m_\varphi^2)^2+\Gamma_\varphi^2 m_\varphi^2}\Big\{-\frac{1}{16}\frac{m_t^3\sqrt{2}G_F}{8\pi^2}\frac{m_t}{-1+\beta^2z^2} \\
&\quad \Big[2\hat{s}(a^2\beta^4-\tilde{a}^2)[{\rm Re}C_0(\hat{s},m_t^2,m_t^2,m_t^2)(\hat{s}-m_\varphi^2) \\
&\quad +{\rm Im}C_0(\hat{s},m_t^2,m_t^2,m_t^2)\Gamma_\varphi m_\varphi]-4a^2\beta^2(\hat{s}-m_\varphi^2)\Big] \\
&\quad +\frac{3}{32}\left(\frac{m_t^3\sqrt{2}G_F}{8\pi^2}\right)^2\Big[\hat{s}^3(a^2\tilde{a}^2\beta^2-\tilde{a}^4)|C_0(\hat{s},m_t^2,m_t^2,m_t^2)|^2 \\
&\quad +\hat{s}(a^4\beta^2-a^2\tilde{a}^2)|2-\hat{s}\beta^2C_0(\hat{s},m_t^2,m_t^2,m_t^2)|^2\Big]\Big\}, \qquad \text{(A.12)}
\end{aligned}
$$

$$
c_{g4} = \frac{g_s^4\beta^2\,(7+9\beta^2z^2)\,(1-z^2)}{32(-1+\beta^2z^2)^2}, \qquad \text{(A.13)}
$$

$$
\begin{aligned}
c_{g5} &= c_{g5,\rm Born} + c_{g5,\rm resonance} \\
c_{g5,\rm Born} &= \frac{g_s^4\beta^2\,(7+9\beta^2z^2)}{96{E_1}^2(E_1+m_t)^2(-1+\beta^2z^2)^2}({E_1}^4+2{E_1}^3m_t-{E_1}^2{m_t}^2 \\
&\quad -4E_1{m_t}^3-2{m_t}^4-2\beta^2{E_1}^3m_tz^2-2\beta^2{E_1}^2{m_t}^2z^2-\beta^4{E_1}^4z^4)
\end{aligned}
$$

$$
\begin{aligned}
c_{g5,\mathrm{resonance}} &= \frac{g_s^4}{(\hat{s}-m_\varphi^2)^2+\Gamma_\varphi^2 m_\varphi^2}\Big\{\frac{1}{16}\frac{m_t^3\sqrt{2}G_F}{8\pi^2}\frac{m_t}{-1+\beta^2z^2} \\
&\Big[4\hat{s}a^2\beta^4[\mathrm{Re}C_0(\hat{s},m_t^2,m_t^2,m_t^2)(\hat{s}-m_\varphi^2) \\
&+\mathrm{Im}C_0(\hat{s},m_t^2,m_t^2,m_t^2)\Gamma_\varphi m_\varphi]-8a^2\beta^2(\hat{s}-m_\varphi^2)\Big] \\
&-\frac{3}{32}\left(\frac{m_t^3\sqrt{2}G_F}{8\pi^2}\right)^2\Big[2\hat{s}^3a^2\tilde{a}^2\beta^2|C_0(\hat{s},m_t^2,m_t^2,m_t^2)|^2 \\
&+2\hat{s}a^4\beta^2|2-\hat{s}\beta^2C_0(\hat{s},m_t^2,m_t^2,m_t^2)|^2\Big]\Big\}, \qquad \text{(A.14)}
\end{aligned}
$$

$$
c_{g6} = \frac{g_s^4\beta^4 z\,(7+9\beta^2z^2)\,(z^2-1)}{96\,(E_1+m_t)\,(-1+\beta^2z^2)^2}. \qquad \text{(A.15)}
$$

The scalar three point function C_0 appearing in equations (A.11), (A.12) and (A.14) is given by

$$
\begin{aligned}
&C_0(\hat{s},m_t^2,m_t^2,m_t^2) = \\
&\int\frac{d^4l}{i\pi^2}\frac{1}{l^2-m_t^2+i\epsilon}\frac{1}{(l-p_1)^2-m_t^2+i\epsilon}\frac{1}{(l-p_1-p_2)^2-m_t^2+i\epsilon}. \qquad \text{(A.16)}
\end{aligned}
$$

Numerically, R^g_{even} is dominated by the Born contributions. This completes our discussion of R^g_{even}.

The CP–violating part R^g_{CP} results from the interference of the Born diagrams with the amplitudes of figs. 1c–1h (with couplings $a\tilde{a}=-\gamma_{CP}$) and the interference of the CP–even and –odd amplitudes of fig. 1h. We found that if m_φ is of the order of $2m_t$ or larger, R^g_{CP} is dominated in the resonance region by the contributions from fig. 1h. Since the complete expressions are rather lengthy, we have split them with respect to the contributions from the individual diagrams. For example, $b^{(\mathrm{h})}_{g2}$ means the contribution from fig. 1h to the function b^{CP}_{g1} and $c^{(\mathrm{d,c})}_{g1}$ denotes the part of c_{g1} that is generated by the diagrams of figs. 1d and 1e.

The function b^{CP}_{g1} gets nonzero contributions only from the box diagrams of fig. 1c:

$$
\begin{aligned}
b^{CP}_{g1} &= b^{(\mathrm{c})}_{g1} = \frac{m_t^3\sqrt{2}G_F\gamma_{CP}}{8\pi^2}\frac{-g_s^4E_1}{96(-1+\beta^2z^2)} \\
&\Big\{(7+9\beta z)\Big[\mathrm{Im}D_s(\hat{t})(1-\beta^2)-2\mathrm{Im}D_{11}(\hat{t})\beta zE_1^2(1-\beta^2) \\
&+2(\mathrm{Im}D_{11}(\hat{t})+\mathrm{Im}D_{21}(\hat{t}))\beta^3zE_1^2(z^2-1)\Big] \\
&+(7-9\beta z)\Big[-\mathrm{Im}D_s(\hat{u})(1-\beta^2)-2\mathrm{Im}D_{11}(\hat{u})\beta zE_1^2(1-\beta^2) \\
&+2(\mathrm{Im}D_{11}(\hat{u})+\mathrm{Im}D_{21}(\hat{u}))\beta^3zE_1^2(z^2-1)\Big]\Big\}. \qquad \text{(A.17)}
\end{aligned}
$$

In this expression,

$$
\begin{aligned}
D_s(\hat{t}) &= D_0(\hat{t})(m_t^2-\hat{t}) + C_0(\hat{s},m_\varphi^2,m_t^2,m_t^2) \\
D_s(\hat{u}) &= D_0(\hat{u})(m_t^2-\hat{u}) + C_0(\hat{s},m_\varphi^2,m_t^2,m_t^2),
\end{aligned}
\tag{A.18}
$$

(where $C_0(\hat{s},m_\varphi,m_t,m_t)$ is defined in (A.7)), $\hat{t}=(p_1-k_1)^2,\ \hat{u}=(p_2-k_1)^2$ and

$$
\begin{aligned}
D_0(\hat{t});D_\mu(\hat{t});D_{\mu\nu}(\hat{t}) &= \int \frac{d^4l}{i\pi^2}\frac{1;l_\mu;l_\mu l_\nu}{l^2-m_\varphi^2+i\epsilon}\frac{1}{(l+k_1)^2-m_t^2+i\epsilon} \\
&\qquad \frac{1}{(l+k_1-p_1)^2-m_t^2+i\epsilon}\frac{1}{(l+k_1-p_1-p_2)^2-m_t^2+i\epsilon} \\
D_\mu(\hat{t}) &= D_{11}(\hat{t})k_{1\mu}-D_{12}(\hat{t})p_{1\mu}-D_{13}(\hat{t})p_{2\mu} \\
D_{\mu\nu}(\hat{t}) &= D_{21}(\hat{t})k_{1\mu}k_{1\nu}+D_{22}(\hat{t})p_{1\mu}p_{1\nu}+D_{23}(\hat{t})p_{2\mu}p_{2\nu} \\
&\quad -D_{24}(\hat{t})k_{1\mu}p_{1\nu}-D_{25}(\hat{t})k_{1\mu}p_{2\nu}+D_{26}(\hat{t})p_{1\mu}p_{2\nu}+D_{27}(\hat{t})g_{\mu\nu}.
\end{aligned}
\tag{A.19}
$$

$D_0(\hat{u});D_\mu(\hat{u});D_{\mu\nu}(\hat{u})$ are obtained from (A.19) by interchanging p_1 and p_2. The functions $D_{11},\ldots,D_{27}$ can be reduced to expressions which contain only the scalar two–, three– and four–point functions $B_0,\ C_0,\ D_0$ (see e.g.[39]).

The function b_{g2}^{CP} reads:

$$
\begin{aligned}
b_{g2}^{CP} &= b_{g2}^{(\mathrm{c})}+b_{g2}^{(\mathrm{g})}+b_{g2}^{(\mathrm{h})} \\
b_{g2}^{(\mathrm{c})} &= \frac{m_t^3\sqrt{2}G_F\gamma_{CP}}{8\pi^2}\frac{g_s^4\beta}{96(-1+\beta^2z^2)} \\
&\quad \Big\{(7+9\beta z)\Big[-\mathrm{Im}D_s(\hat{t})\frac{m_t}{E_1+m_t}(E_1+m_t+\beta zE_1) \\
&\quad +2\mathrm{Im}D_{11}(\hat{t})m_tE_1(-E_1+E_1z^2-m_tz^2)+4\mathrm{Im}D_{27}(\hat{t})m_t \\
&\quad +2(\mathrm{Im}(D_{11}\hat{t})+\mathrm{Im}D_{21}(\hat{t}))\beta^2E_1^2(z^2-1)(2m_t+E_1z^2-m_tz^2)\Big] \\
&\quad +(7-9\beta z)\Big[-\mathrm{Im}D_s(\hat{u})\frac{m_t}{E_1+m_t}(E_1+m_t-\beta zE_1) \\
&\quad +2\mathrm{Im}D_{11}(\hat{u})m_tE_1(-E_1+E_1z^2-m_tz^2)+4\mathrm{Im}D_{27}(\hat{u})m_t \\
&\quad +2(\mathrm{Im}D_{11}(\hat{u})+\mathrm{Im}D_{21}(\hat{u}))\beta^2E_1^2(z^2-1)(2m_t+E_1z^2-m_tz^2)\Big]\Big\} \\
b_{g2}^{(\mathrm{g})} &= \frac{m_t^3\sqrt{2}G_F\gamma_{CP}}{8\pi^2}\frac{3g_s^4m_t\beta^3z^2\mathrm{Im}G(\hat{s})}{8(-1+\beta^2z^2)}
\end{aligned}
$$

$$
\begin{aligned}
b_{g2}^{(\mathrm{h})} &= \frac{1}{(\hat{s}-m_\varphi^2)^2+\Gamma_\varphi^2 m_\varphi^2}\frac{m_t^3\sqrt{2}G_F\gamma_{CP}}{8\pi^2}\frac{g_s^4 m_t\beta}{4(-1+\beta^2z^2)} \\
&\quad \Big\{2m_t^2\Big[\mathrm{Re}C_0(\hat{s},m_t^2,m_t^2,m_t^2)\Gamma_\varphi m_\varphi \\
&\quad -\mathrm{Im}C_0(\hat{s},m_t^2,m_t^2,m_t^2)(\hat{s}-m_\varphi^2)\Big]+\Gamma_\varphi m_\varphi\Big\}. \qquad \text{(A.20)}
\end{aligned}
$$

As can be seen seen explicitly from these formulae, all contributions to the functions b_{g1}^{CP} and b_{g2}^{CP} result either from absorptive parts of the one loop amplitudes or from terms of the form: width Γ_φ times dispersive terms (which is present only in $b_{g2}^{(\mathrm{h})}$). This is in agreement with the general statements made in section 2. One can also check the relations following from Bose symmetry as given in table 1. The functions c_{g1} and c_{g2} arise from dispersive parts in the one loop amplitude or width terms times absorptive parts (which is present only in $c_{g2}^{(\mathrm{h})}$ below). They read:

$$
\begin{aligned}
c_{g1} &= c_{g1}^{(\mathrm{c})}+c_{g1}^{(\mathrm{d,e})}+c_{g1}^{(\mathrm{f})} \\
c_{g1}^{(\mathrm{c})} &= \frac{m_t^3\sqrt{2}G_F\gamma_{CP}}{8\pi^2}\frac{-g_s^4E_1}{96(-1+\beta^2z^2)} \\
&\quad \Big\{(7+9\beta z)\Big[\mathrm{Re}D_s(\hat{t})(1-\beta^2)-2\mathrm{Re}D_{11}(\hat{t})\beta z E_1^2(1-\beta^2) \\
&\quad -2(\mathrm{Re}D_{11}(\hat{t})+\mathrm{Re}D_{21}(\hat{t}))\beta^3 z E_1^2(z^2-1)\Big] \\
&\quad +(7-9\beta z)\Big[-\mathrm{Re}D_s(\hat{u})(1-\beta^2)-2\mathrm{Re}D_{11}(\hat{u})\beta z E_1^2(1-\beta^2) \\
&\quad -2(\mathrm{Re}D_{11}(\hat{u})+\mathrm{Re}D_{21}(\hat{u}))\beta^3 z E_1^2(z^2-1)\Big]\Big\} \\
c_{g1}^{(\mathrm{d,e})} &= \frac{m_t^3\sqrt{2}G_F\gamma_{CP}}{8\pi^2}\frac{-g_s^4E_1}{96(-1+\beta^2z^2)} \\
&\quad \Big\{(9\beta z+7)\Big[2C_0(\hat{t},m_\varphi^2,m_t^2,m_t^2)(\beta^2-1) \\
&\quad +\frac{\beta z}{\beta z-1}C_s(\hat{t})(\beta^2z^2-2\beta^2+1)\Big] \\
&\quad +(9\beta z-7)\Big[2C_0(\hat{u},m_\varphi^2,m_t^2,m_t^2)(\beta^2-1) \\
&\quad +\frac{\beta z}{\beta z+1}C_s(\hat{u})(\beta^2z^2-2\beta^2+1)\Big]\Big\} \\
c_{g1}^{(\mathrm{f})} &= \frac{m_t^3\sqrt{2}G_F\gamma_{CP}}{8\pi^2}\frac{-g_s^4}{192E_1(-1+\beta^2z^2)} \\
&\quad \Big\{(7+9\beta z)(B_0(m_t^2,m_\varphi^2,m_t^2)-B_0(\hat{t},m_\varphi^2,m_t^2))\frac{\beta^2-1}{\beta z-1} \\
&\quad +(7-9\beta z)(B_0(m_t^2,m_\varphi^2,m_t^2)-B_0(\hat{u},m_\varphi^2,m_t^2))\frac{\beta^2-1}{\beta z+1}\Big\}, \qquad \text{(A.21)}
\end{aligned}
$$

where we used the notation

$$C_s(\hat{t}) = C_0(\hat{t}, m_\varphi^2, m_t^2, m_t^2) + \frac{B_0(m_t^2, m_\varphi^2, m_t^2) - B_0(\hat{t}, m_\varphi^2, m_t^2)}{m_t^2 - \hat{t}}$$
$$C_s(\hat{u}) = C_0(\hat{u}, m_\varphi^2, m_t^2, m_t^2) + \frac{B_0(m_t^2, m_\varphi^2, m_t^2) - B_0(\hat{u}, m_\varphi^2, m_t^2)}{m_t^2 - \hat{u}}, \quad \text{(A.22)}$$

and

$$C_0(\hat{t}, m_\varphi^2, m_t^2, m_t^2) =$$
$$\int \frac{d^4l}{i\pi^2} \frac{1}{l^2 - m_\varphi^2 + i\epsilon} \frac{1}{(l+k_1)^2 - m_t^2 + i\epsilon} \frac{1}{(l+k_1-p_1)^2 - m_t^2 + i\epsilon}. \quad \text{(A.23)}$$

$C_0(\hat{u}, m_\varphi^2, m_t^2, m_t^2)$ is obtained from (A.23) by the replacement $p_1 \to p_2$.
Finally,

$$\begin{aligned}
c_{g2} &= c_{g2}^{(\mathrm{c})} + c_{g2}^{(\mathrm{d,e})} + c_{g2}^{(\mathrm{f})} + c_{g2}^{(\mathrm{g})} + c_{g2}^{(\mathrm{h})}, \\
c_{g2}^{(\mathrm{c})} &= \frac{m_t^3\sqrt{2}G_F\gamma_{CP}}{8\pi^2} \frac{-g_s^4\beta}{96(-1+\beta^2z^2)} \\
&\quad \Big\{(7+9\beta z)\Big[-\mathrm{Re}D_s(\hat{t}) \frac{m_t}{E_1+m_t}(E_1 + m_t - \beta z E_1) \\
&\quad +2\mathrm{Re}D_{11}(\hat{t}) m_t E_1 (E_1 - E_1 z^2 + m_t z^2) + 4\mathrm{Re}D_{27}(\hat{t}) m_t \\
&\quad +2(\mathrm{Re}D_{11}(\hat{t}) + \mathrm{Re}D_{21}(\hat{t}))\beta^2 E_1^2 (z^2-1)(2m_t + E_1 z^2 - m_t z^2)\Big] \\
&\quad +(7-9\beta z)\Big[-\mathrm{Re}D_s(\hat{u}) \frac{m_t}{E_1+m_t}(E_1 + m_t + \beta z E_1) \\
&\quad +2\mathrm{Re}D_{11}(\hat{u}) m_t E_1 (E_1 - E_1 z^2 + m_t z^2) + 4\mathrm{Re}D_{27}(\hat{u}) m_t \\
&\quad +2(\mathrm{Re}D_{11}(\hat{u}) + \mathrm{Re}D_{21}(\hat{u}))\beta^2 E_1^2 (z^2-1)(2m_t + E_1 z^2 - m_t z^2)\Big]\Big\} \\
c_{g2}^{(\mathrm{d,e})} &= \frac{m_t^3\sqrt{2}G_F\gamma_{CP}}{8\pi^2} \frac{-g_s^4\beta}{96(-1+\beta^2z^2)} \\
&\quad \Big\{(7+9\beta z)\Big[2C_0(\hat{t}, m_\varphi^2, m_t^2, m_t^2) \frac{m_t}{E_1+m_t}(E_1 + m_t - \beta z E_1) \\
&\quad +C_s(\hat{t}) \frac{-m_t - E_1 z^2 + m_t z^2}{E_1^2(1-\beta z)}(E_1^2 - 2m_t^2 - \beta^2 E_1^2 z^2)\Big] \\
&\quad +(7-9\beta z)\Big[2C_0(\hat{u}, m_\varphi^2, m_t^2, m_t^2) \frac{m_t}{E_1+m_t}(E_1 + m_t + \beta z E_1) \\
&\quad +C_s(\hat{u}) \frac{-m_t - E_1 z^2 + m_t z^2}{E_1^2(1+\beta z)}(E_1^2 - 2m_t^2 - \beta^2 E_1^2 z^2)\Big]\Big\}
\end{aligned}$$

$$
\begin{aligned}
c_{g2}^{(\mathrm{f})} &= \frac{m_t^3\sqrt{2}G_F\gamma_{CP}}{8\pi^2}\frac{g_s^4}{192(-1+\beta^2z^2)} \\
&\Big\{(7+9\beta z)(B_0(m_t^2,m_\varphi^2,m_t^2)-B_0(\hat{t},m_\varphi^2,m_t^2)) \\
&\frac{m_t}{E_1+m_t}\frac{E_1+m_t-\beta zE_1}{E_1^2(1-\beta z)} \\
&+(7-9\beta z)(B_0(m_t^2,m_\varphi^2,m_t^2)-B_0(\hat{u},m_\varphi^2,m_t^2)) \\
&\frac{m_t}{E_1+m_t}\frac{E_1+m_t+\beta zE_1}{E_1^2(1+\beta z)}\Big\} \\
c_{g2}^{(\mathrm{g})} &= \frac{m_t^3\sqrt{2}G_F\gamma_{CP}}{8\pi^2}\frac{-3g_s^4m_t\beta^3z^2\mathrm{Re}G(\hat{s})}{8(-1+\beta^2z^2)} \\
c_{g2}^{(\mathrm{h})} &= \frac{g_s^4\gamma_{CP}}{(\hat{s}-m_\varphi^2)^2+\Gamma_\varphi^2m_\varphi^2}\Big\{-\frac{1}{16}\frac{m_t^3\sqrt{2}G_F}{8\pi^2}\frac{m_t\beta}{-1+\beta^2z^2} \\
&\Big[2\hat{s}(1+\beta^2)[\mathrm{Re}C_0(\hat{s},m_t^2,m_t^2,m_t^2)(\hat{s}-m_\varphi^2) \\
&+\mathrm{Im}C_0(\hat{s},m_t^2,m_t^2,m_t^2)\Gamma_\varphi m_\varphi]-4(\hat{s}-m_\varphi^2)\Big] \\
&+\frac{3}{32}\left(\frac{m_t^3\sqrt{2}G_F}{8\pi^2}\right)^2[2\hat{s}^3\beta\tilde{a}^2|C_0(\hat{s},m_t^2,m_t^2,m_t^2)|^2 \\
&+2\hat{s}\beta a^2|2-\hat{s}\beta^2C_0(\hat{s},m_t^2,m_t^2,m_t^2)|^2]\Big\}. \qquad \text{(A.24)}
\end{aligned}
$$

References

[1] L. Rolandi: Talk given at 26th International Conference on High Energy Physics (ICHEP 92) Dallas, 6-12 August 1992, published in Dallas HEP (1992) 56.

[2] F. Abe et al. (CDF Collaboration) FERMILAB-CONF-93-212-E, to appear in Proc. of 16th International Symposium on Lepton and Photon Interactions, Ithaca, NY, 10-15 August 1993.

[3] M. Kobayashi, T. Maskawa: Progr. Theor. Phys. **49** (1973) 652.

[4] N. Turok, J. Zadrozny: Nucl. Phys. **B 358** (1991) 471; L. McLerran, M.E. Shaposhnikov, N. Turok, M. Voloshin: Phys. Lett. **B 256** (1991) 451; M. Dine, P. Huet, R. Singleton, L. Susskind: Phys. Lett. **B 257** (1991) 351; A. Nelson, A. Cohen, D. Kaplan: Nucl. Phys. **B 373** (1992) 453.

[5] T.D. Lee: Phys. Rev. **D 8** (1973); Phys. Rep. **9** (1974) 143; S. Weinberg: Phys. Rev. Lett. **37** (1976) 657; P. Sikivie, Phys. Lett. **B 65** (1976) 141; H.B. Lahanas, C.E. Vayonakis: Phys. Rev. **D 19** (1979) 2158; G.C. Branco, A.J. Buras, J.M. Gérard: Nucl. Phys. **B 259** (1985) 306; J. Liu, L. Wolfenstein: Nucl. Phys. **B 289** (1987) 1.

[6] G.C. Branco, M.N. Rebelo: Phys. Lett. **B 160** (1985) 117; S. Weinberg: Phys. Rev. **D 42** (1990) 860.

[7] N.G. Deshpande, E. Ma: Phys. Rev. **D 16** (1977) 1583.

[8] W. Bernreuther, T. Schröder, T.N. Pham: Phys. Lett. **B 279** (1992) 389.

[9] B. Grzadkowski, J. Gunion: Phys. Lett. **B 289** (1992) 440.

[10] C.R. Schmidt, M.E. Peskin: Phys. Rev. Lett. **69** (1992) 410.

[11] W. Bernreuther, A. Brandenburg: Phys. Lett. **B 314** (1993) 104

[12] J.F. Donoghue, G. Valencia: Phys. Rev. Lett. **58** (1987) 451; **59** (1988) 243 (E).

[13] C.A. Nelson: Phys. Rev. **D 41** (1990) 2805

[14] W. Bernreuther, O. Nachtmann: Phys. Lett. **B 268** (1991) 424.

[15] G.L. Kane, G.A. Landinsky, C.-P. Yuan: Phys. Rev. **D 45** (1991) 124.

[16] W. Bernreuther, O. Nachtmann, P. Overmann, T. Schröder: Nucl. Phys. **B 388** (1992) 53; **B 406** (1993) 516 (E).

[17] D. Atwood, A. Soni: Phys. Rev. **D 45** (1992) 2405; D. Atwood, A. Aeppli, A. Soni: Phys. Rev. Lett. **69** (1992) 2754; D. Atwood, G. Eilam, A. Soni: Phys. Rev. Lett. **71** (1993) 492.

[18] J.P. Ma, A. Brandenburg: Z. Phys. **C 56** (1992) 97; A. Brandenburg, J.P. Ma: Phys. Lett. **B 298** (1993) 211.

[19] C.R. Schmidt: Phys. Lett. **B 293** (1992) 111.

[20] B. Grzadkowski: Phys. Lett. **B 305** (1993) 384; B. Grzadkowski, W.-Y. Keung: CERN preprint CERN-TH.6917/93 (1993)

[21] W. Bernreuther, P. Overmann: Heidelberg preprint HD-THEP-93-11 (1993).

[22] J. Liu: Phys. Rev. **D 47** (1993) R1741

[23] A. Pilaftsis, M. Nowakoski: Mainz preprint MZ-TH-92-56 (1992).

[24] D. Chang, W.-Y. Keung: Phys. Lett. **B 305** (1993) 261.

[25] D. Chang, W.-Y. Keung, I. Phillips: CERN preprint CERN-TH-6658.92-REV (1993).

[26] K.F. Smith et al.: Phys. Lett. **B 234** (1990) 191.

[27] S.A. Murthy et al.: Phys. Rev. Lett. **63** (1989) 965; K. Abdullah et al.: Phys. Rev. Lett. **65** (1990) 2347.

[28] X.G. He, J.P. Ma, B. McKellar: Melbourne preprint UM-P-93-11 (1993); Phys. Lett. **B 304** (1993) 285.

[29] A. Mendez, A. Pomarol: Phys. Lett. **B 272** (1991) 313.

[30] J.F. Gunion, T.C. Yuan, B. Grzadkowski: Phys. Rev. Lett. **71** (1993) 488.

[31] A. Ilakovac, B.A. Kniehl, A. Pilaftsis: preprint MAD-PH-787 (1993).

[32] A. Djouadi, B.A. Kniehl: preprint UDEM-LPN-TH-93-171 (1992).

[33] C. Kao: Florida preprint FSU-HEP-930924 (1993).

[34] J. Kühn: Acta Phys. Austriaca Suppl. XXIV (1982) 203; I. Bigi, Y. Dokshitzer, V. Khoze, J. Kühn, P. Zerwas: Phys. Lett. **B 181** (1986) 157.

[35] A. Czarnecki, M.Jezabek, J.H. Kühn: Nucl. Phys. **B 351** (1991) 70.

[36] G.A. Ladinsky: Phys. Rev. **D 46** (1992) 3789; **D 47** (1993) 3086 (E).

[37] J.F. Owens: Phys. Lett. **B 266** (1991) 126.

[38] G. 't Hooft, M. Veltman: Nucl. Phys. **B 153** (1979) 365.

[39] G. Pasarino, M. Veltman: Nucl. Phys. **B 160** (1979) 151.

Table Caption

Table 1: Transformation properties of the structure functions defined in (2.2)–(2.3).

Table 1

	CP	P	T ($\mathrm{Im}\mathcal{T}=0$)	CPT ($\mathrm{Im}\mathcal{T}=0$)	"Bose"
$A^g(z)$	$A^g(z)$	$A^g(z)$	$A^g(z)$	$A^g(z)$	$A^g(-z)$
$b^{\pm}_{g1}(z)$	$b^{\mp}_{g1}(z)$	$-b^{\pm}_{g1}(z)$	$b^{\pm}_{g1}(z)$	$b^{\mp}_{g1}(z)$	$-b^{\pm}_{g1}(-z)$
$b^{\pm}_{g2}(z)$	$b^{\mp}_{g2}(z)$	$-b^{\pm}_{g2}(z)$	$b^{\pm}_{g2}(z)$	$b^{\mp}_{g2}(z)$	$b^{\pm}_{g2}(-z)$
$b^{\pm}_{g3}(z)$	$b^{\mp}_{g3}(z)$	$b^{\pm}_{g3}(z)$	$-b^{\pm}_{g3}(z)$	$-b^{\mp}_{g3}(z)$	$-b^{\pm}_{g3}(-z)$
$c_{g0}(z)$	$c_{g0}(z)$	$c_{g0}(z)$	$c_{g0}(z)$	$c_{g0}(z)$	$c_{g0}(-z)$
$c_{g1}(z)$	$-c_{g1}(z)$	$-c_{g1}(z)$	$-c_{g1}(z)$	$c_{g1}(z)$	$-c_{g1}(-z)$
$c_{g2}(z)$	$-c_{g2}(z)$	$-c_{g2}(z)$	$-c_{g2}(z)$	$c_{g2}(z)$	$c_{g2}(-z)$
$c_{g3}(z)$	$-c_{g3}(z)$	$c_{g3}(z)$	$c_{g3}(z)$	$-c_{g3}(z)$	$-c_{g3}(-z)$
$c_{g4}(z)$	$c_{g4}(z)$	$c_{g4}(z)$	$c_{g4}(z)$	$c_{g4}(z)$	$c_{g4}(-z)$
$c_{g5}(z)$	$c_{g5}(z)$	$c_{g5}(z)$	$c_{g5}(z)$	$c_{g5}(z)$	$c_{g5}(-z)$
$c_{g6}(z)$	$c_{g6}(z)$	$c_{g6}(z)$	$c_{g6}(z)$	$c_{g6}(z)$	$-c_{g6}(-z)$
$c_{g7}(z)$	$c_{g7}(z)$	$-c_{g7}(z)$	$-c_{g7}(z)$	$-c_{g7}(z)$	$c_{g7}(-z)$
$c_{g8}(z)$	$c_{g8}(z)$	$-c_{g8}(z)$	$-c_{g8}(z)$	$-c_{g8}(z)$	$-c_{g8}(-z)$

Figure Captions

Fig. 1: Born level QCD and φ exchange Feynman diagrams which contribute to the production density matrix for $gg \to t\bar{t}$. Diagrams with crossed gluons are not shown.

Fig. 2: Born level QCD and relevant φ exchange Feynman diagrams for $q\bar{q} \to t\bar{t}$.

Fig. 3: Expectation value $\langle \hat{\mathbf{k}} \cdot (\mathbf{s}_+ - \mathbf{s}_-) \rangle_g$ as a function of the parton CM energy for $m_\varphi = 100$ GeV (dashed curve) and $m_\varphi = 350$ GeV (solid curve).

Fig. 4: Expectation value $\langle \hat{\mathbf{k}} \cdot (\mathbf{s}_+ \times \mathbf{s}_-) \rangle_g$ for the same choice of Higgs masses as in Fig. 3.

Fig. 5: Same as Fig. 3, but for $\langle \hat{\mathbf{k}} \cdot (\mathbf{s}_+ - \mathbf{s}_-) \rangle_q$.

Fig. 6: Same as Fig. 4, but for $\langle \hat{\mathbf{k}} \cdot (\mathbf{s}_+ \times \mathbf{s}_-) \rangle_q$.

Fig. 7: Signal–to–noise ratio for the observable A_1 (defined in (4.1)) as a function of the Higgs boson mass m_φ for proton–proton CM energies $\sqrt{s} = 15$ TeV (solid curve) and $\sqrt{s} = 40$ TeV (dashed curve). Here $m_t = 150$ GeV, $a = -\tilde{a} = 1$, $\hat{g}_{VV} = 1$.

Fig. 8: Same as fig. 7, but for the observable A_2 (defined in (4.2)).

Fig. 9: Same as fig. 7, but for the observable T_2 (defined in (4.3)).

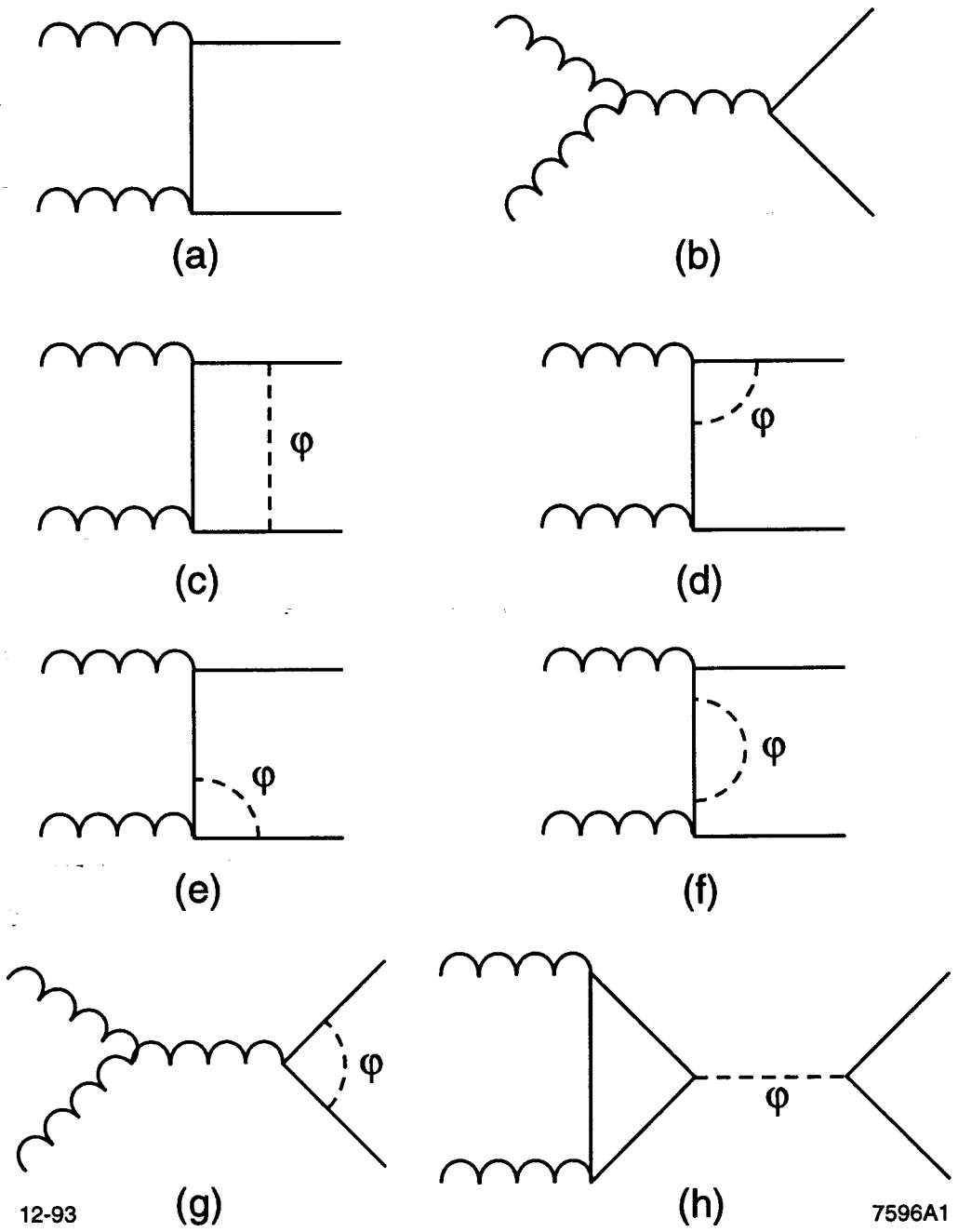

Fig. 1

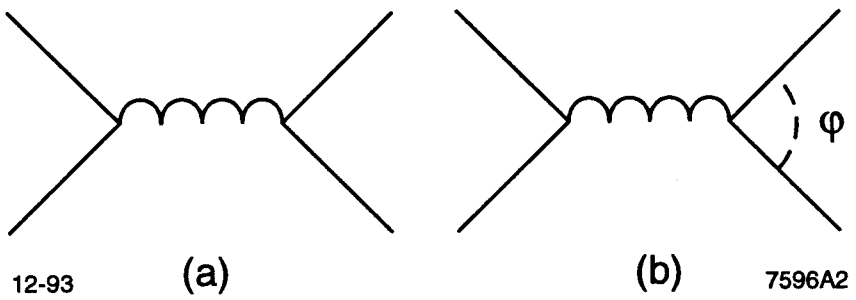

Fig. 2

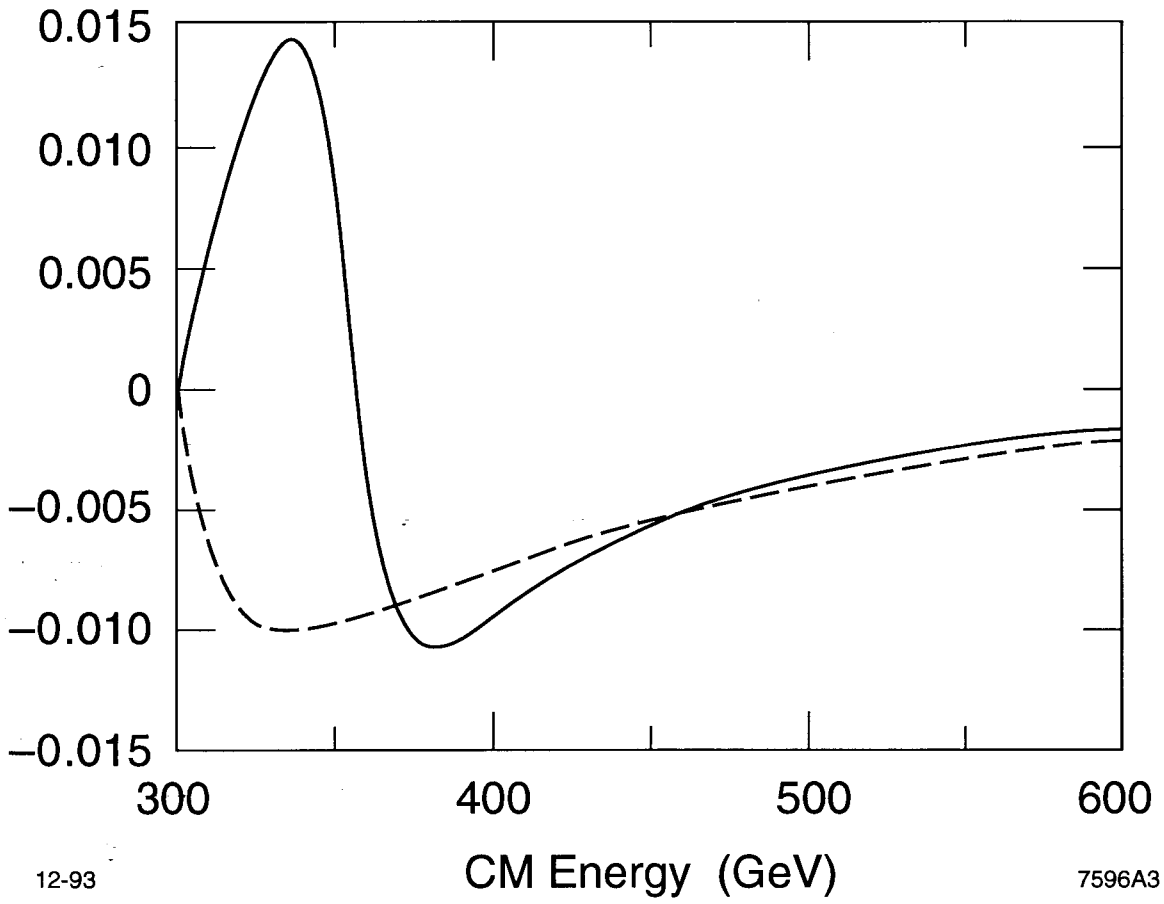
0.015
0.010
0.005
0
−0.005
−0.010
−0.015
300
400
500
600
CM Energy (GeV)
12-93
7596A3

Fig. 3

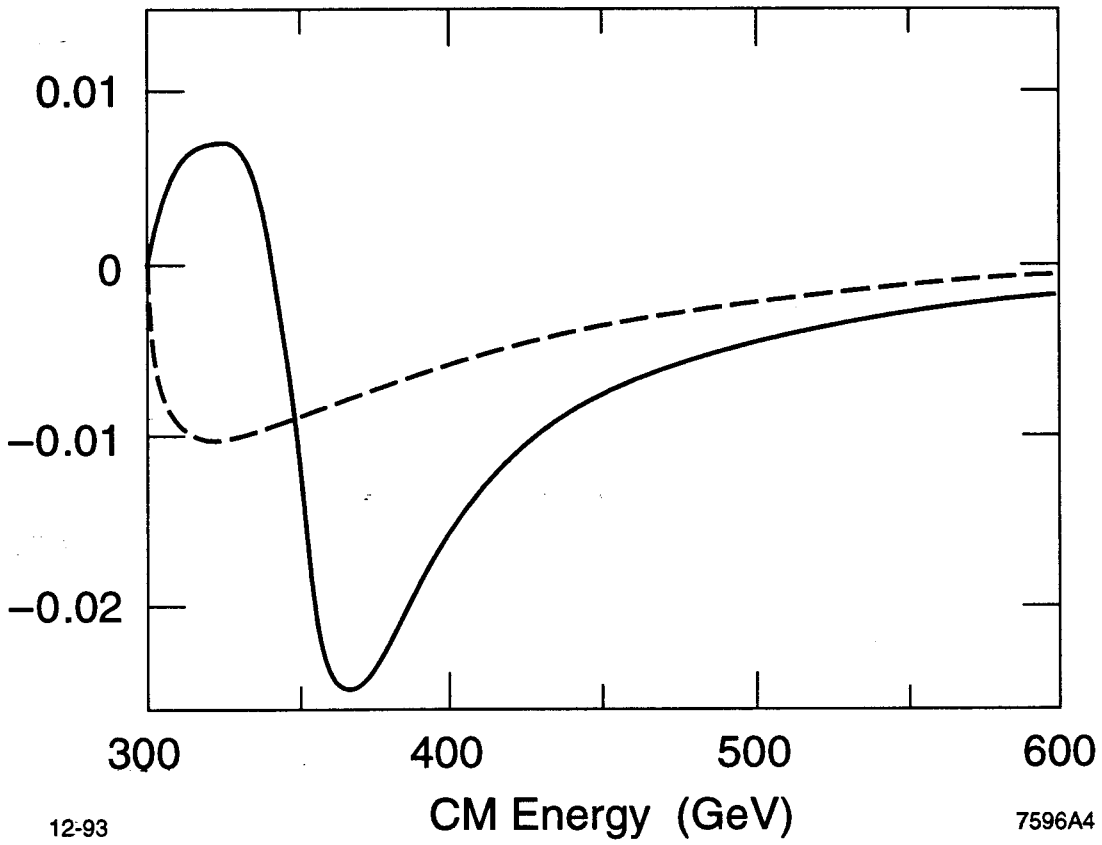

Fig. 4

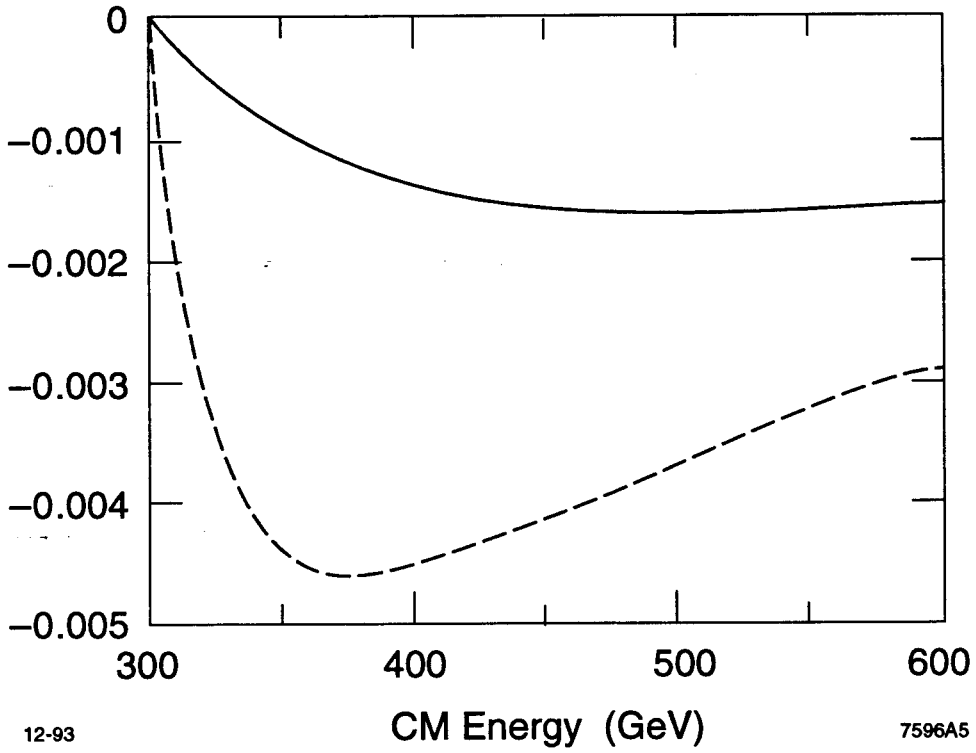
0
−0.001
−0.002
−0.003
−0.004
−0.005
300
400
500
600
CM Energy (GeV)
12-93
7596A5

Fig. 5

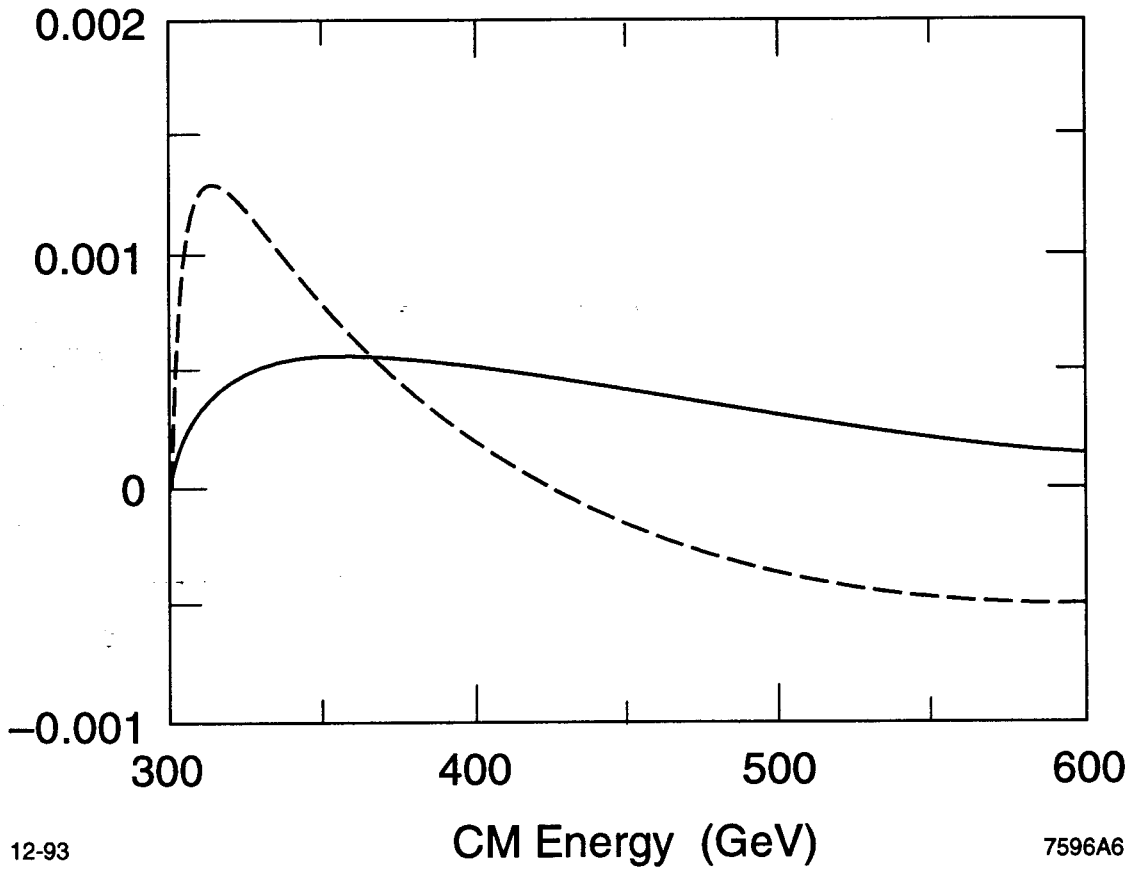

Fig. 6

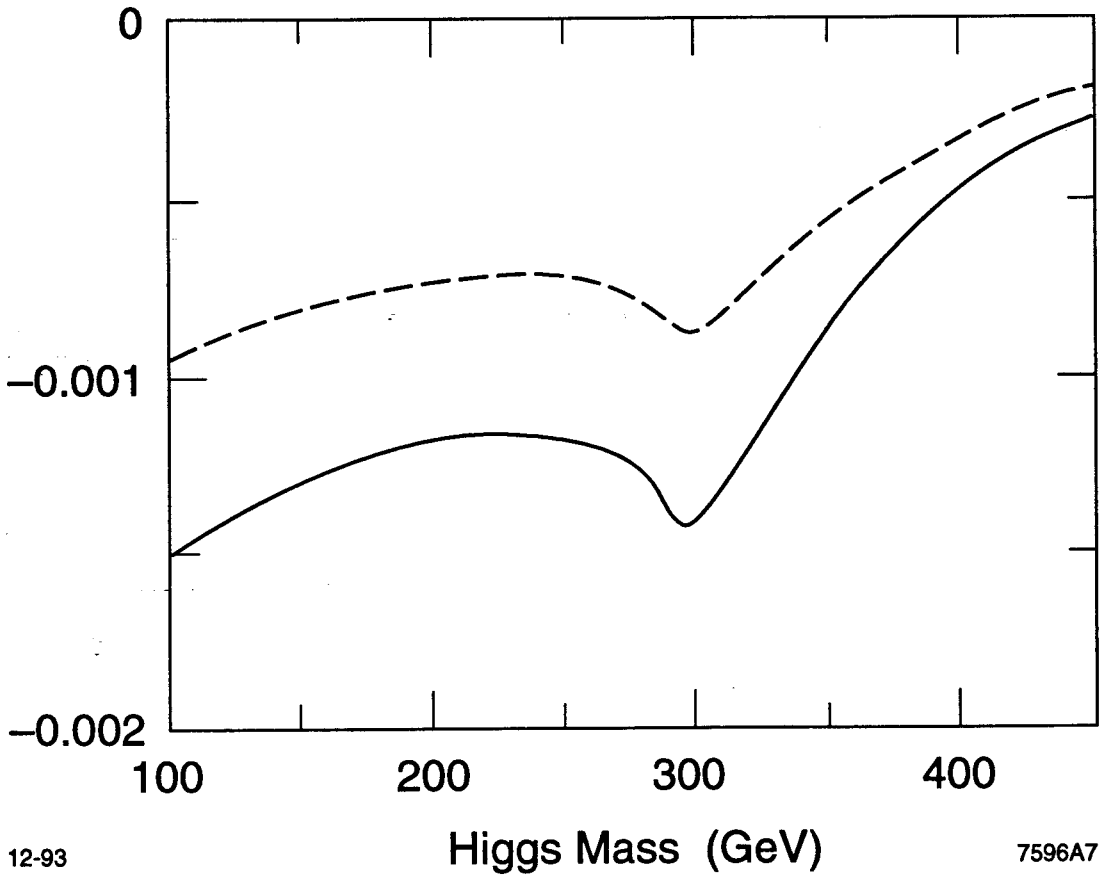

Fig. 7

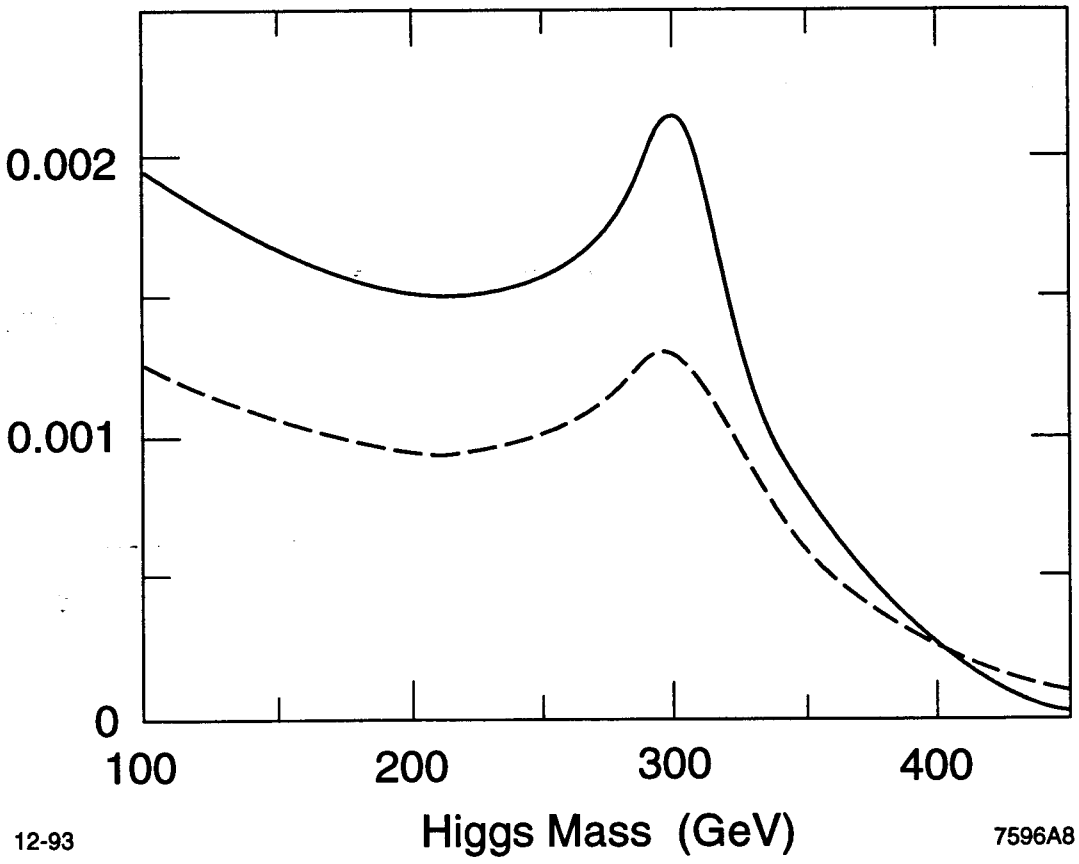

Fig. 8

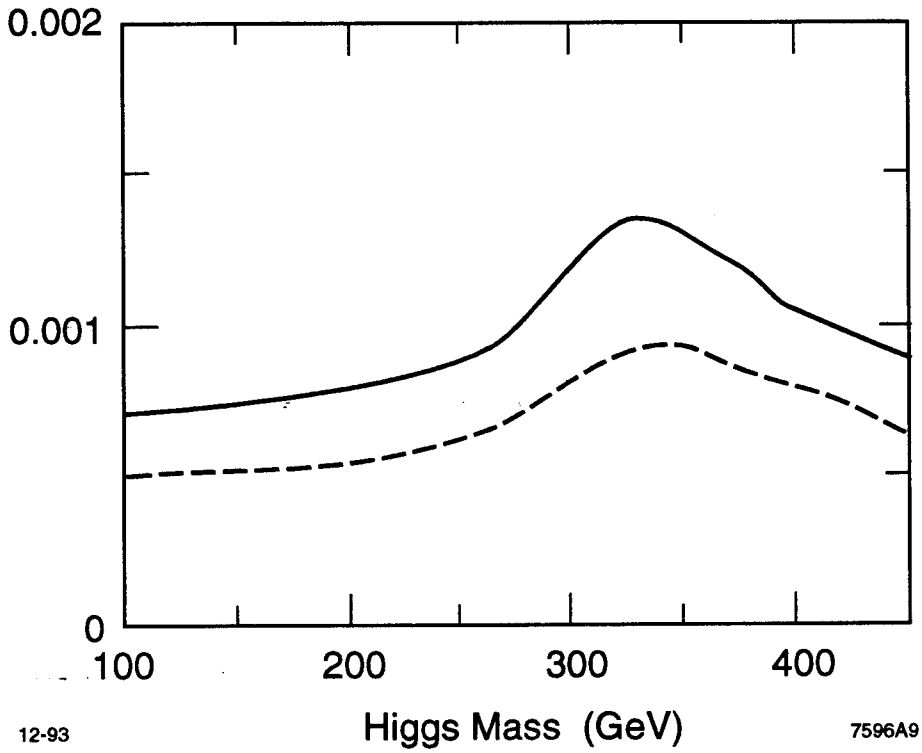

Fig. 9